Modeling of thermal contacts with heat generation: Application to electrothermal problems

Anas El Maakoul, Benjamin Remy, Alain Degiovanni

▶ **To cite this version:**

Anas El Maakoul, Benjamin Remy, Alain Degiovanni. Modeling of thermal contacts with heat generation: Application to electrothermal problems. International Journal of Heat and Mass Transfer, 2019, 140, pp.293-302. 10.1016/j.ijheatmasstransfer.2019.06.015 . hal-02441295

HAL Id: hal-02441295

https://hal.univ-lorraine.fr/hal-02441295v1

Submitted on 25 Oct 2021

HAL is a multi-disciplinary open access archive for the deposit and dissemination of scientific research documents, whether they are published or not. The documents may come from teaching and research institutions in France or abroad, or from public or private research centers.

L'archive ouverte pluridisciplinaire **HAL**, est destinée au dépôt et à la diffusion de documents scientifiques de niveau recherche, publiés ou non, émanant des établissements d'enseignement et de recherche français ou étrangers, des laboratoires publics ou privés.

Distributed under a Creative Commons Attribution - NonCommercial 4.0 International License

Version of Record: https://www.sciencedirect.com/science/article/pii/S0017931019303485
Manuscript_2e6baee27f80a68b59186b8405e656b5

Modeling of thermal contacts with heat generation: application to electrothermal problems

Anas El Maakoul [b*], Benjamin Remy [a], Alain Degiovanni [a,b]
[a] Université de Lorraine, CNRS, LEMTA, 54504 cedex, Vandoeuvre les Nancy, France
[b] Université Internationale de Rabat, Pôle Energie, LERMA, 11100 Sala Al Jadida, Maroc

Abstract:

When modeling thermal contacts with heat generation between two solids (e.g. electrothermal applications), we are often interested in evaluating the heat transfer rates and contact temperatures, and generally, it is difficult to evaluate these thermal characteristics due to interfacial conditions. In this work, a general representation of solid-solid thermal contact problems with heat generation is proposed. This representation is based on the thermal-electrical analogy and uses the notion of partition coefficient β. The resulting equivalent thermal circuits are presented and discussed. The pertinence of this analytical approach is demonstrated for the electrothermal application of Joule heating for different contact configurations (similar and dissimilar materials, with and without interstitial fluid). The analytical results for each configuration are compared to numerical results obtained using numerical simulations under similar conditions, both results are in very good agreement.

1. Introduction:

Modeling thermal contacts problems with heat generation is both complex and difficult. This difficulty comes mainly from modeling the interfacial conditions, and until now, to the authors knowledge, there is no model or method that received unanimous acceptance by the heat transfer community.

In the literature, there are numerous studies where different models are proposed and applied to various applications of thermal contacts with heat generation. Depending on the application, two mains categories can be identified: Contacts with friction (molding, machining, …) and electrothermal contacts (electrical conductors, spot welding process …).

A description of representative studies that appear in the literature now follows. For the first category of contacts with friction, several research works dealt with machining and molding [1-4], while in others, the authors studied dry contact under perfect contact conditions [5-10] or Imperfect contact conditions [11-14]. The heat generated through friction was evaluated differently depending on the authors. Some distributed the heat sources [15,16], some located the heat generation on the contact plane [17], others located it on one of the friction surfaces [18]. Other authors, based on the approach used by Bardon [19], considered interfacial heat generation using the notion of 'part of the generated heat that causes a spike in temperature at the interface' or 'heat generation factor' [20-24]. As for the second category of electrothermal contacts, heat is generated in the matter of the materials in contact. There are various models for this category, such as with or without contact resistance and with or without interfacial heat generation [25-33].

The foregoing short introduction shows that the main difficulty lies in the representation of the heat sources, particularly if we want to keep the notion of "contact resistance". One representation that can be generalized was introduced by Bardon [19] which, as mentioned previously, consists in considering interfacial heat generation and introducing a heat generation factor α, the equivalent thermal circuit for this representation in shown in figure 1. In this case, R_1 and R_2 are respectively the non-perturbed thermal resistances of mediums 1 and 2, R_c is the contact resistance and φ_g the total rate of heat generation.

© 2019 published by Elsevier. This manuscript is made available under the CC BY NC user license
https://creativecommons.org/licenses/by-nc/4.0/

In this representation, the coefficient α depends not only on the spatial distribution of the heat sources but also on the thermal conductivities λ_1 and λ_2 of the mediums 1 and 2. Another problem with this representation is that does not permit the evaluation of the contact temperature.

In this paper, we consider the solid-solid thermal contact problem with heat generation and propose a general representation, that is easily applicable, to evaluate the heat transfer rates and contact temperature. To do so, we first need to examine in detail the notion of "contact resistance".

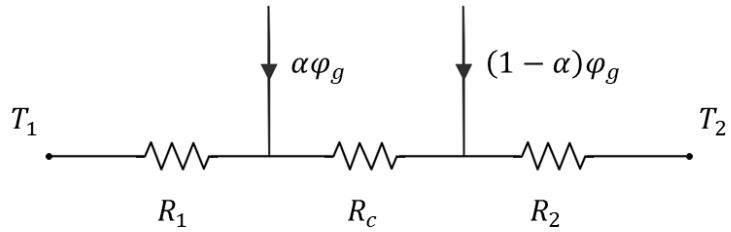

Figure 1: Equivalent thermal circuit proposed by Bardon [19]

2. Concept of "contact resistance":

Let's consider the contact between two solids without heat sources (figure 2), because the solid contact spots are interspersed with gaps (that are generally filled with a fluid), the actual contact area (solid contact spots) is much smaller than the apparent area. The contact resistance is described using an axisymmetric elementary contact cell that corresponds to a reference contact area associated to a rate of heat transfer; the overall contact and heat transfer are represented by multiple elementary cells in parallel [34, 35] as shown in figure 2. Figure 3 represents schematically an elementary cell.

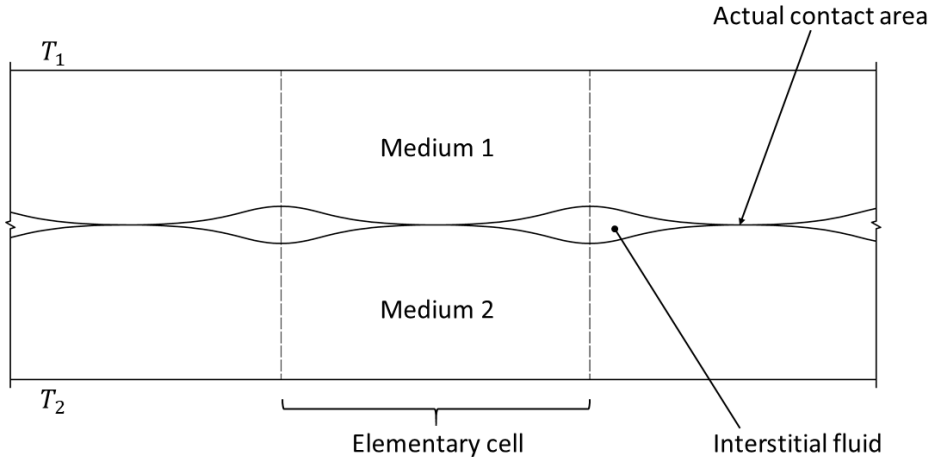

Figure 2: Representation of contact between two solids

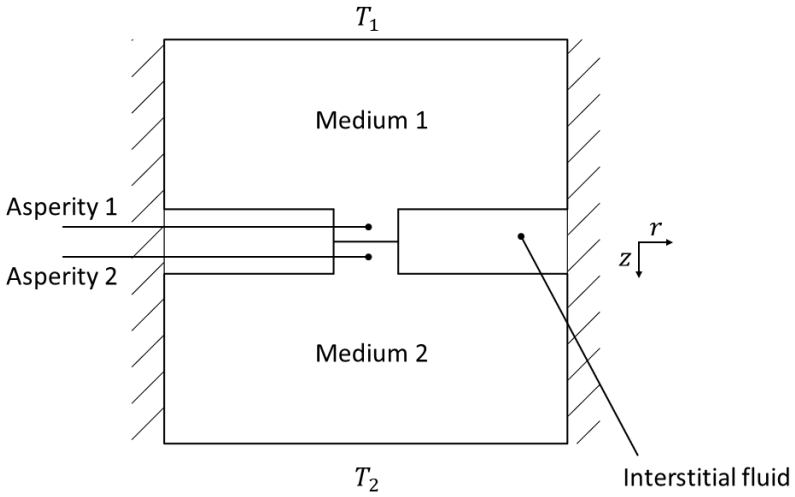

Figure 3: schematic representation of an axisymmetric elementary contact cell

With reference to figure 3, the rigorous approach consists in splitting the elementary cell into two parallel heat transfer regions (internal and external). In the internal region, heat flows through the asperities while in the external region heat flows though the interstitial fluid. The foregoing is presented in figure 4.a, where the two regions are separated with dashed curves.

Noting that the total heat transfer is the sum of the heat transfer rates ϕ_i and ϕ_e, we can write:

$$\frac{1}{R_t} = \frac{1}{R_i} + \frac{1}{R_e} \tag{1}$$

Where R_t is the total thermal resistance, R_i and R_e are respectively the thermal resistances of the internal and external regions. Let's decompose the resistance of each region into resistances connected in series (figure 4.b and figure 5):

$$R_i = R_{m1i} + R_{c1i} + R_{a1} + R_{a2} + R_{c2i} + R_{m2i} \tag{2}$$

$$R_e = R_{m1e} + R_{c1e} + R_f + R_{c2e} + R_{m2e} \tag{3}$$

Where

- R_{m1i} and R_{m2i} represent the resistances associated to the surface S_i (internal region).
- R_{m1e} and R_{m2e} represent the resistances associated to the surface S_e (external region).
- R_{a1} and R_{a2} are the resistance of the asperities.
- R_f is the resistance of the fluid
- R_{c1i} and R_{c2i} are the constriction resistances associated to the internal region (narrowing heat flow area, see figure 4)
- R_{c1e} and R_{c2e} are the constriction resistances associated to the external region (widening heat flow area)

a)

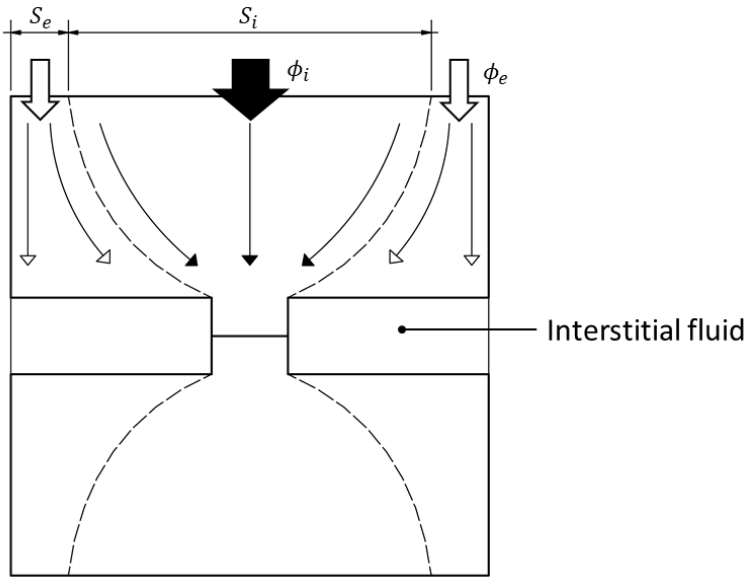

b)

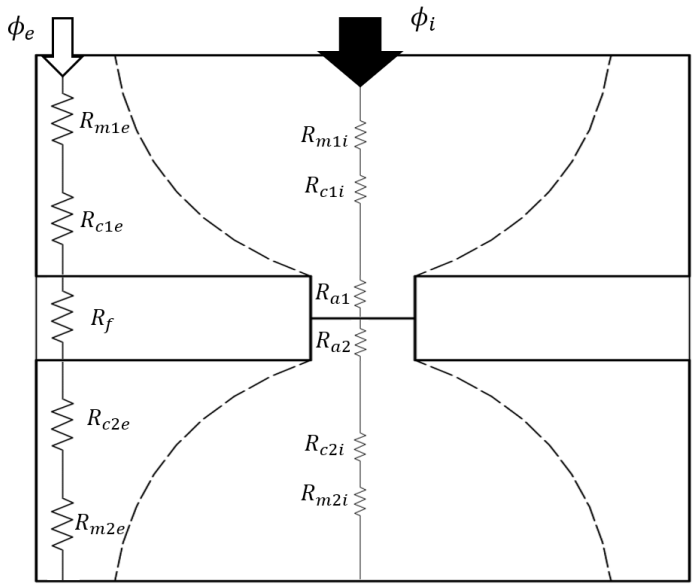

Figure 4: a) internal (ϕ_i) and external (ϕ_e) heat transfer regions for an elementary cell; b) thermal resistances in series for each region (Eq (2-3))

In figure 5, it can be demonstrated (see appendix 1) that the potentials A and C are the identical, the same is true for the potentials B and D. Moreover, in most cases, the actual contact area is much smaller than the apparent area, therefore the external constriction resistances (R_{c1e} and R_{c2e}) are negligible compared to the fluid resistance R_f and the internal constriction resistances are very close to the intrinsic constriction resistances (irrespective of the asperities and the fluid) [36]. The inferred thermal circuit is shown in figure 6 where R_c is the contact resistance.

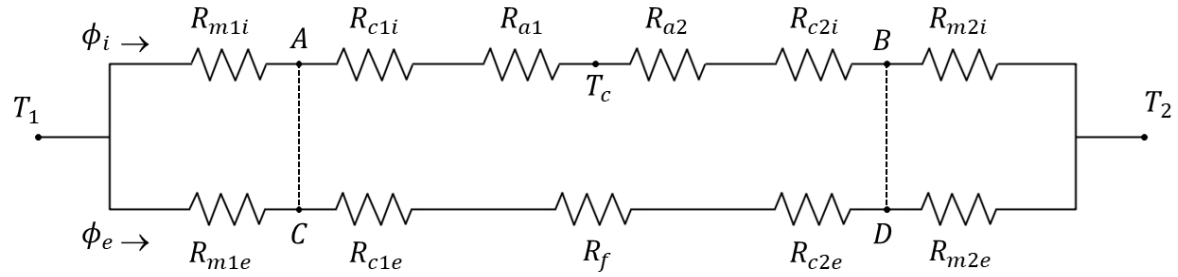

Figure 5: The complet equivalent thermal circuit for contact problems without heat source

82

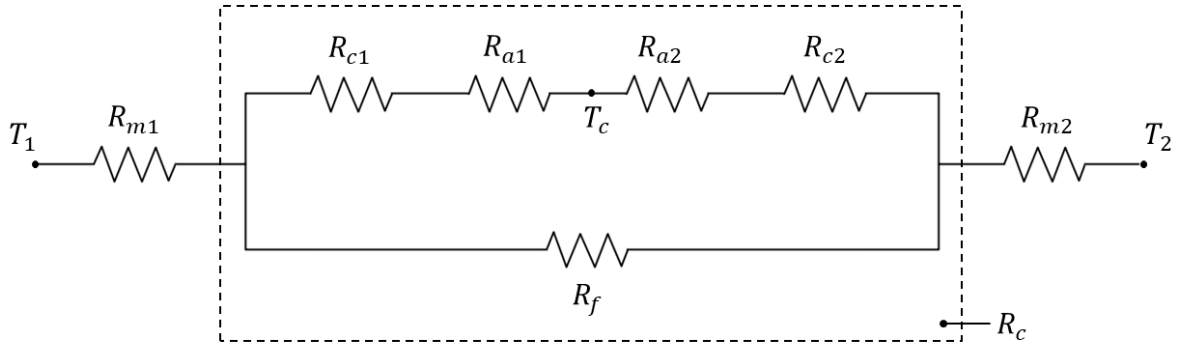

Figure 6: Simplified equivalent thermal circuit for contact problems without heat source

83

84 Can the preceding equivalent thermal circuit be modified to consider internal heat sources? in the case
85 of localized sources, the problem is solved by simply applying Kirchhoff's current law, while for a
86 distributed source (heat generation varying with position), it was demonstrated that the problem has
87 an equivalent thermal circuit [37]. In the next section, we briefly present this demonstration for the
88 special case of curvilinear coordinates.

89 **3. Notion of partition coefficient in a steady conduction problem with an internal source [37]:**

90 Let's consider the case of unidirectional conduction with internal sources where the heat flux vector is
91 perpendicular to the isothermal surfaces. The sources are uniform between two isotherms and we can
92 define a curvilinear coordinate s orthogonal to the isotherms (figure 7).

93 With $g(s)$ the volumetric heat generation rate, $S(s)$ the isothermal section and constant thermo-
94 physical properties, we can write Fourier's equation as:

$$\phi(s) = -\lambda\, S(s) \frac{dT(s)}{ds} \tag{4}$$

95 And the energy balance:

$$d\phi = g(s)S(s)ds \tag{5}$$

96 We define:

$$Q = \int_{s_{in}}^{s_{out}} g(s)S(s)ds \qquad r(s) = \int_{s_{in}}^{s} \frac{ds}{\lambda S(s)} \qquad R = \int_{s_{in}}^{s_{out}} \frac{ds}{\lambda S(s)}$$

97

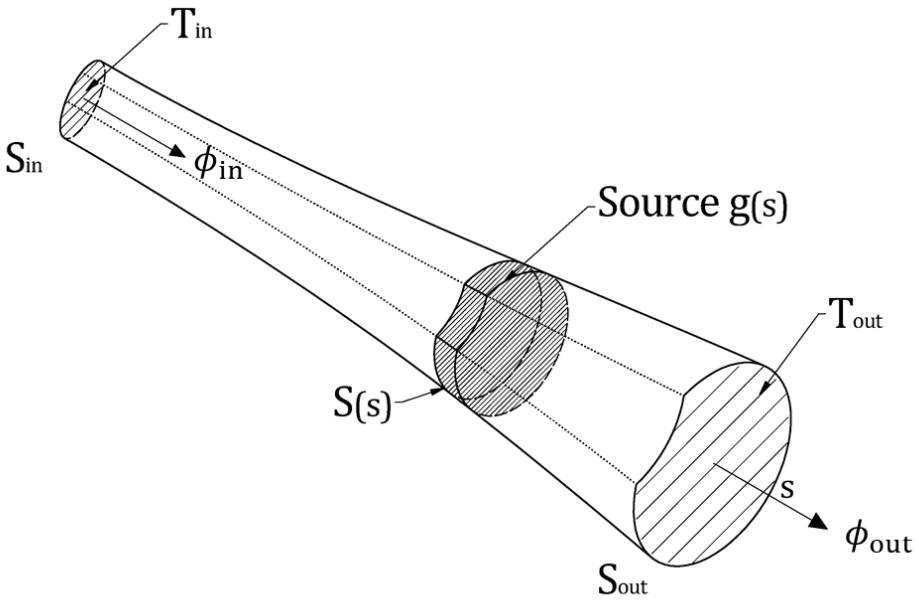

Figure 7: Unidirectional conduction with internal sources

Integrating equation (5) from s_{in} to s_{out}, we get:

$$\phi_{out} = Q + \phi_{in} \tag{6}$$

Integrating equation (4) from s_{in} to s_{out} yields:

$$T_{in} - T_{out} = R\phi_{out} - \int_{s_{in}}^{s_{out}} r(s)g(s)S(s)ds \tag{7}$$

As demonstrated in [37], relations (6) and (7) correspond to the thermal circuit shown in figure 8, which shows that a medium with an internal heat source can be represented using an equivalent thermal circuit with two resistances βR and $(1-\beta)R$, where the total rate of heat generation Q is dissipated between the two resistances. Therefore:

$$\beta = \int_{s_{in}}^{s_{out}} \frac{r(s)}{R}\frac{g(s)}{Q}\, S(s)ds \tag{8}$$

β is the partition coefficient and Q is the total rate of heat generation in the medium.

In this representation, β is independent of the medium's thermal conductivity and is only a function of the source's distribution.

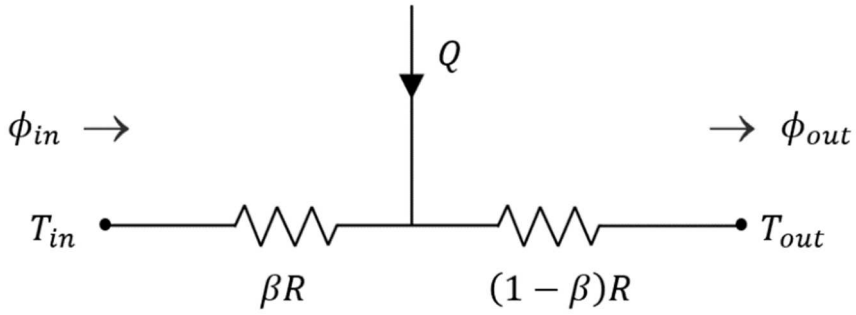

Figure 8: Equivalent thermal circuit of heat conduction in a medium with an internal heat source

4. Application to electrothermal problems:

With reference to figure 7, we consider the problem of heat generation due to Joule heating which represents the conversion from electrical to thermal energy in a current-carrying medium. An electric potential difference is imposed between S_{in} and S_{out}, thus an electric current I flows through the medium. Considering ρ_e the electrical resistivity of the medium, the electrical resistance of an element ds is expressed in the same way as the thermal resistance (solution of the same problem, $\Delta T = 0$ or $\Delta V = 0$, for the same volume and boundary conditions):

$$dr_e = \frac{\rho_e ds}{S(s)}$$

Thus

$$g(s) = \frac{\rho_e ds}{S(s)} I^2 \frac{1}{S(s)ds} = \frac{\rho_e I^2}{S^2(s)} \tag{9}$$

Relation (8) becomes:

$$\beta = \int_{s_{in}}^{s_{out}} \frac{\int_{s_{in}}^{s} \frac{ds}{\lambda S(s)}}{\int_{s_{in}}^{s_{out}} \frac{ds}{\lambda S(s)}} \frac{\frac{\rho_e I^2}{S^2(s)}}{\int_{s_{in}}^{s_{out}} \frac{\rho_e I^2}{S^2(s)} S(s)ds} S(s)ds \tag{10}$$

Which reduces to

$$\beta = \int_{s_{in}}^{s_{out}} \frac{\int_{s_{in}}^{s} \frac{ds}{S(s)} \cdot \frac{ds}{S(s)}}{\left(\int_{s_{in}}^{s_{out}} \frac{ds}{S(s)}\right)^2} \tag{11}$$

Let $F(s) = \int_{s_{in}}^{s} \frac{ds}{S(s)}$ (with $F(s_{in}) = 0$), we get:

$$\beta = \frac{1}{F^2(s_{out})} \int_{s_{in}}^{s_{out}} F(s)F'(s)ds = \frac{1}{2} \tag{12}$$

The partition coefficient β is a constant equal to $1/2$. This remarkable result can be demonstrated for the general electrothermal problem (steady or transient) with any geometrical configuration (see [37]).

5. Thermal contact with heat sources:

Let's consider the circuit shown in figure 5. In the presence of heat sources in the internal and external branches, the potentials A and C are no longer identical and the same is true for potentials B and D. This prevents, in the general case, the definition of the contact resistance.

Let's consider the two following particular cases.

5.1. Fluid with a high thermal resistance:

An example is the thermal contact in a vacuum environment. For this case, the circuit in figure 5 reduces to one branch (internal) with heat sources and we can use the preceding result shown in figure 8. The thermal equivalent circuit for this case is shown in figure 10 where:

$$R_1 = R_{m1} + R_{c1} + R_{a1}$$

And

$$R_2 = R_{m2} + R_{c2} + R_{a2}$$

R_1 and R_2 are respectively the total thermal resistances of medium 1 and 2. T_c is the contact temperature. Note that in the circuit of figure 10, the only approximation is that the contact is isothermal.

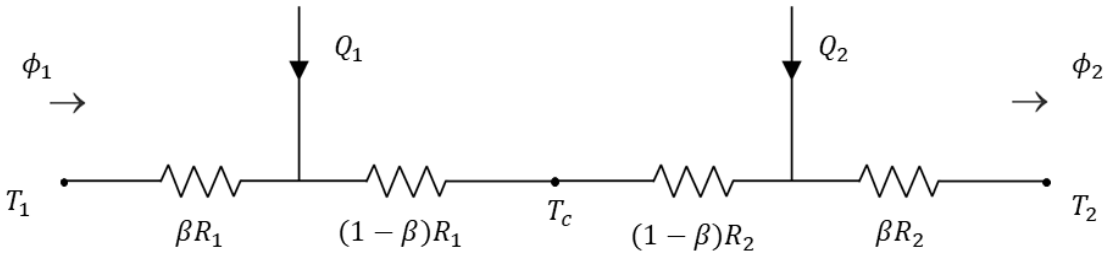

Figure 10: Equivalent thermal circuit of thermal contact with heat source and $R_f \to \infty$

5.2. Fluid with a non-negligible thermal resistance:

In this case, the solution is obtained by exploiting the linearity of the problem. The temperature is then written in the form $T = X + Y$. For the problem in X, there is a temperature difference ($T_1 \neq T_2$) with no heat source, while for the problem in Y, there is a heat source without temperature difference ($T_1 = T_2$). The solution to the problem in X is given by figure 6. The solution to the problem in Y can be simplified if we assume that the heat transfer through the external region is negligible (this hypothesis will be later verified using numerical simulations), thus, the solution to the problem in Y is given by figure 10 where $T_1 = T_2 = 0$. The equivalent thermal circuits for this case are shown in figure 11.

The heat transfer rates are:

$$\phi_1 = \phi_X + \phi_{Y1} \tag{13}$$

$$\phi_2 = \phi_X + \phi_{Y2} \tag{14}$$

And the contact temperature

$$T_c = X_c + Y_c \tag{15}$$

For electrothermal problems, we only need to use $\beta = 1/2$.

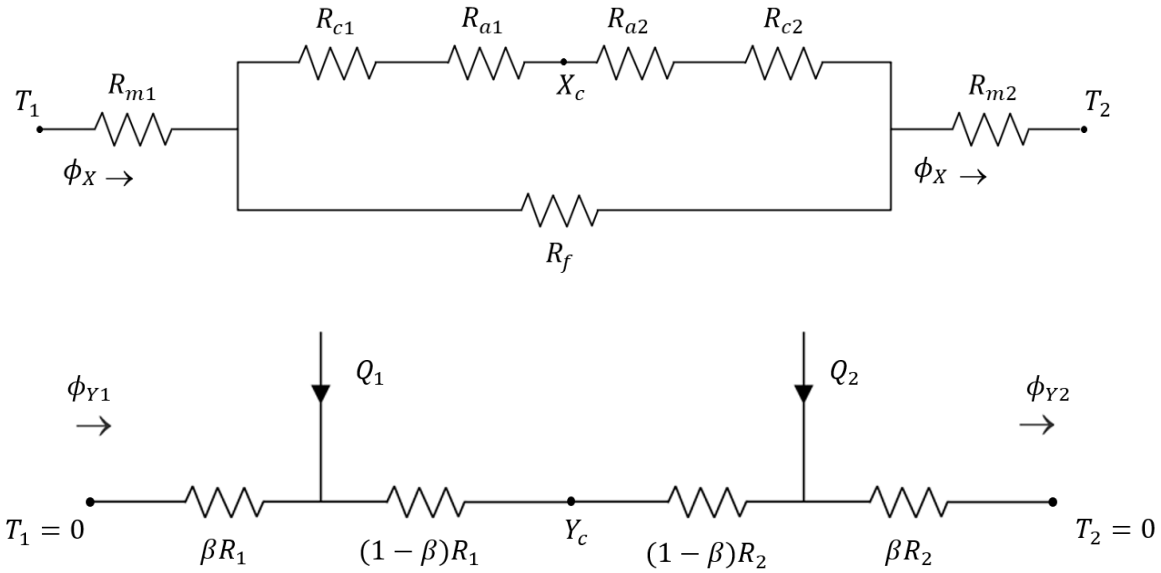

Figure 11: Equivalent thermal circuit for thermal contacts with heat source and interstitial fluid

6. Numerical simulations and comparison to the macroscopic approach: application to an elementary contact cell

In this section, the results of the analytical approach are compared to numerical simulations for the elementary contact cell described in figure 12. The height l_1 and l_2 are sufficiently larger than the radius a so that the constriction is fully developed; the radius b is sufficiently small as to obtain a realistic model.

The geometrical parameters are:

$$a = 10\ \mu m\ ; b = 1\ \mu m\ ; l_1 = l_2 = 20\ \mu m$$

Two materials are considered, Iron and Copper, the interstitial fluid is air. The relevant physical properties are listed below:

- Iron: $\lambda = 40\ Wm^{-1}\ K^{-1}$ and $\rho_e = 10^{-7}\ \Omega m$
- Copper: $\lambda = 400\ Wm^{-1}\ K^{-1}$and $\rho_e = 2 \cdot 10^{-8}\ \Omega m$
- Air: $\lambda_f = 0.025\ Wm^{-1}\ K^{-1}$ and $\rho_e = 1.24 \cdot 10^{14}\ \Omega m$

We define three interface configurations:

- Configuration 1: Asperities with nil thickness $\delta_1 = \delta_2 = 0$ without any interstitial fluid
- Configuration 2: Asperities of thickness $\delta_1 = \delta_2 = 0.5\ \mu m$ without interstitial fluid
- Configuration 3: Asperities of thickness $\delta_1 = \delta_2 = 0.5\ \mu m$ with air as interstitial fluid

And four different cases:

- Case 1: iron to iron contact with $T_1 = T_2 = 0°C$ and $\Delta U = 4.24 \cdot 10^{-2}\ V$
- Case 2: iron to copper contact with $T_1 = T_2 = 0°C$ and $\Delta U = 4.24 \cdot 10^{-2}\ V$
- Case 3: iron to iron contact with $T_1 = 100°C$, $T_2 = 0°C$ and $\Delta U = 4.24 \cdot 10^{-2}\ V$
- Case 4: iron to copper contact with $T_1 = 100°C$, $T_2 = 0°C$ and $\Delta U = 4.24 \cdot 10^{-2}\ V$

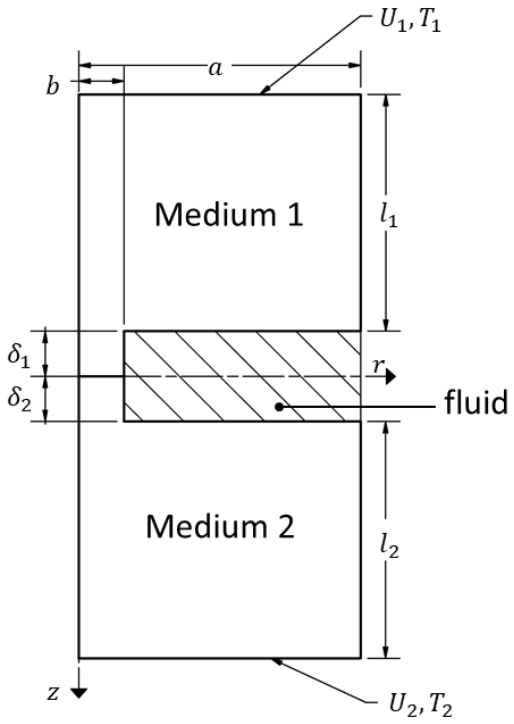

Figure 12: Thermal contact with heat source in an axisymmetric elementary cell

6.1. Numerical results:

The numerical simulations are carried out using FLUENT, the geometry is modeled exploiting its axisymmetry. The computational domains are meshed with triangle and quadrilateral elements. the conformal mesh is locally refined at the interface. For each case, a mesh sensitivity test was conducted where the optimal mesh is adopted. The energy and electric potential equations are iteratively solved. The convergence was judged by monitoring residuals and key quantities such as the temperature and potential at the interface (T_c and U_c). The numerical results are summarized in table 1.

Table 1: Numerical results				
Configuration 1: Asperities with nil thickness $\delta_1 = \delta_2 = 0$				
Parameter	Case 1	Case 2	Case 3	Case 4
	Iron	Iron	Iron	Iron
	Iron	Copper	Iron	Copper
$\Delta U\ (V)$	0.0424	0.0424	0.0424	0.0424
ΔT	0	0	100	100
$\phi_1(W)$	-0.01595	-0.02475	-0.00893	-0.01175
$\phi_2(W)$	0.01596	0.02884	0.02323	0.04185
$U_c(V)$	0.0212	0.0072	0.0212	0.0072
$T_c(°C)$	55.41	17.04	106.25	26.14
$I\ (A)$	0.76	1.26	0.76	1.26
Configuration 2: Asperities of thickness $\delta_1 = \delta_2 = 0.5\ \mu m$ without interstitial fluid				
Parameter	Case 1	Case 2	Case 3	Case 4
	Iron	Iron	Iron	Iron
	Iron	Copper	Iron	Copper
$\Delta U\ (V)$	0.0424	0.0424	0.0424	0.0424
ΔT	0	0	100	100
$\phi_1(W)$	-0.01000	-0.01541	-0.00555	-0.00732
$\phi_2(W)$	0.01000	0.01793	0.01445	0.02603
$U_c(V)$	0.0212	0.0071	0.0212	0.0071
$T_c(°C)$	56.17	17.03	106.19	26.12
$I\ (A)$	0.47	0.79	0.47	0.79
Configuration 3: Asperities of thickness $\delta_1 = \delta_2 = 0.5\ \mu m$ with air as interstitial fluid				
Parameter	Case 1	Case 2	Case 3	Case 4
	Iron	Iron	Iron	Iron
	Iron	Copper	Iron	Copper
$\Delta U\ (V)$	0.0424	0.0424	0.0424	0.0424
ΔT	0	0	100	100
$\phi_1(W)$	-0.00993	-0.01519	-0.00495	-0.00659
$\phi_2(W)$	0.00993	0.01800	0.01491	0.02659
$U_c(V)$	0.0212	0.0072	0.0212	0.0072
$T_c(°C)$	56.31	17.69	106.31	27.15
$I\ (A)$	0.47	0.78	0.47	0.78

6.2. Calculation of thermal resistances:

R_{m1}, R_{m2}, R_{a1}, R_{a2} and R_f are wall type resistances, that is, they take the form $e/\lambda S$ where e is the wall thickness, λ its conductivity and S the heat transfer area. R_{c1} and R_{c2} are the constrictions resistances and depend on the boundary condition at the contact interface. The classical approach [38] shows that there are two limiting conditions that correspond to 'uniform heat flux' and 'uniform

temperature'. The analytical solutions obtained in the form of series were approximated and presented in a practical manner by various authors, here we will use the following formulas proposed in [38]:

Uniform temperature
$$R_c = \frac{1}{4\lambda r} f\left(\frac{r}{R}\right) \tag{16}$$

Uniform heat flux
$$R_c = \frac{8}{3\pi^2 \lambda r} f\left(\frac{r}{R}\right) \tag{17}$$

With

$$f\left(\frac{r}{R}\right) = 1 - 1.288\frac{r}{R} + 0.288\left(\frac{r}{R}\right)^{3.75}$$

In the following we will show that the deviation between the analytical and numerical results comes solely from the approximate calculation of the constriction resistances. We will also use the resistances obtained using numerical simulations.

6.3. Configuration 1: Asperities with nil thickness $\delta_1 = \delta_2 = 0$:

6.3.1. Thermal resistances

The thermal resistances values for Iron are presented below, in K/W. For copper, the resistances can be obtained by dividing the values below by 10 ($\lambda_{copper}/\lambda_{iron} = 10$).

R_m	R_a	R_c (Analytical calculations for a uniform heat flux)	R_c (Analytical calculations for a uniform temperature)	R_c (Numerical simulations)
1591.5	0	5885	5445	5400

6.3.2. Analytical-numerical comparison

In this configuration, the interface temperature is uniform as demonstrated in [35] and confirmed by the numerical results as shown in figure 13. The numerical temperature at $z = \delta_1$ is plotted against the radius ($0 \leq r \leq b$). The small deviations are caused by the singularity at $r = b$.

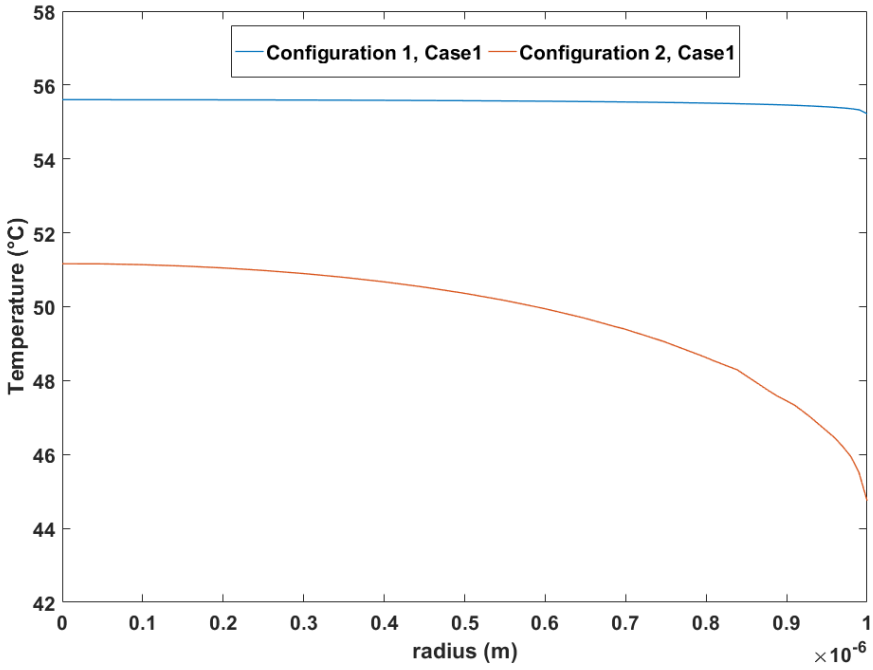

Figure 13: Temperature profile at $z = \delta_1$ for configuration 1, case 1 and configuration 2, case 1.

The overall results for this configuration are summarized in table 2. The 'analytical-numerical' method is about using the analytical approach with the numerically obtained thermal resistances. The 'analytical-analytical' method uses the analytical approach with the constriction resistance evaluated through equations (16) and (17), the first and second lines contain respectively the results for a 'uniform temperature' and a 'uniform heat flux' interfacial boundary conditions. The detailed calculations are presented in appendix 2.

Table 2: Numerical and analytical comparison for configuration 1: Asperities with nil thickness

Method	Parameter		Case 1 Iron-Iron	Case 2 Iron-Copper	Case 3 Iron-Iron	Case 4 Iron-Copper
Numerical	$\phi_1(mW)$		-15.95	-24.75	-8.93	-11.75
	$\phi_2(mW)$		15.96	28.84	23.23	41.85
	$T_c(°C)$		55.40	17.04	106,2	26.14
Numerical-Analytical	$\phi_1(mW)$		-16.06	-24.74	-8.91	-11.74
	$\phi_2(mW)$		16.06	28.81	23.21	41.80
	$T_c(°C)$		56.1	17.02	106.1	26.11
Analytical-Analytical	$\phi_1(mW)$	Eq (16)	-16.06	-24.73	-8.95	-11.82
		Eq (17)	-16.06	-24.74	-9.37	-12.58
	$\phi_2(mW)$	Eq (16)	16.06	28.81	23.77	41.72
		Eq (17)	16.06	28.81	22.75	40.96
	$T_c(°C)$	Eq (16)	56.5	17.13	106.5	26.22
		Eq (17)	60.0	18.20	110.9	27.29

From the foregoing, it is clear that there is a good agreement between the numerical and analytical 'uniform temperature' approach, for both the heat transfer rates and interface temperatures.

6.4. Configuration 2: Asperities of thickness $\boldsymbol{\delta_1 = \delta_2 = 0.5\ \mu m}$ without interstitial fluid:

6.4.1. Thermal resistances

The thermal resistances values for Iron are reported below, in K/W. For copper, the resistances can be obtained by dividing the values below by 10 ($\lambda_{copper}/\lambda_{iron} = 10$).

R_m	R_a	R_c (Analytical calculations for a uniform heat flux)	R_c (Analytical calculations for a uniform temperature)	R_c (Numerical simulations)
1591.5	3978.8	5885	5445	5664.31

6.4.2. Analytical-numerical comparison

In this configuration, the temperature at $z = \delta_1$ is not uniform (see figure 13). This is also confirmed from the preceding values for the contact resistances where the numerical contact resistance is between the two analytical contact resistances.

The results are presented in table 3, there is a perfect analytical-numerical agreement by using the numerical constriction resistances in the analytical calculations. When using the analytical constriction resistances in the analytical calculations, the maximum relative deviation is less than 2%.

Table 3: Numerical and analytical comparison for configuration 2: Asperities of thickness $\delta_1 = \delta_2 = 0.5\ \mu m$ without interstitial fluid						
Method	Parameter		Case 1	Case 2	Case 3	Case 4
			Iron-Iron	Iron-Copper	Iron-Iron	Iron-Copper
Numerical	$\phi_1(mW)$		-10.00	-15.41	-5.55	-7.32
	$\phi_2(mW)$		10.00	17.93	14.45	26.03
	$T_c(°C)$		56.17	17.03	106.2	26.12
Numerical-Analytical	$\phi_1(mW)$		-10.00	-15.40	-5.55	-7.31
	$\phi_2(mW)$		10.00	17.93	14.45	26.02
	$T_c(°C)$		56.16	17.02	106.1	26.11
Analytical-Analytical	$\phi_1(mW)$	Eq (16)	-10.00	-15.40	-5.46	-7.15
		Eq (17)	-10.00	-15.40	-5.63	-7.46
	$\phi_2(mW)$	Eq (16)	10.00	17.93	14.54	26.18
		Eq (17)	10.00	17.93	14.36	25.86
	$T_c(°C)$	Eq (16)	55.07	16.69	105.0	25.78
		Eq (17)	57.27	17.35	107.3	26.44

6.5. Configuration 3: Asperities of thickness $\delta_1 = \delta_2 = 0.5\ \mu m$ with air as interstitial fluid

6.5.1. Thermal resistances

The thermal resistances values for Iron are reported below, in K/W. For copper, the resistances can be obtained by dividing the values below by 10 ($\lambda_{copper}/\lambda_{iron} = 10$).

R_m	R_a	R_f	R_c (Analytical calculations for a uniform heat flux)	R_c (Analytical calculations for a uniform temperature)	R_c Numerical simulations
1591.5	3978.8	128610	5885	5445	5664.31

6.5.2. Analytical-numerical comparison

Here, the analytical calculations are done using the superposition principle as shown in section 4.2 and represented in figure 11 with $\beta = 1/2$.

The results for this configuration are reported in table 4. There is a good analytical-numerical agreement. Taking the numerical results as a reference, the numerical-analytical and analytical-analytical methods have maximum deviations of less than 1% and 4% respectively.

Table 4: Numerical and analytical comparison for configuration 2: Asperities of thickness $\delta_1 = \delta_2 = 0.5\ \mu m$ with air as interstitial fluid						
Method	Parameter		Case 1	Case 2	Case 3	Case 4
			Iron-Iron	Iron-Copper	Iron-Iron	Iron-Copper
Numerical	$\phi_1(mW)$		-9.93	-15.19	-4.95	-6.59
	$\phi_2(mW)$		9.93	18.00	14.91	26.59
	$T_c(°C)$		56.31	17.69	106.3	27.15
Numerical-Analytical	$\phi_1(mW)$		-9.91	-15.26	-4.90	-6.60
	$\phi_2(mW)$		9.91	17.76	14.92	26.42
	$T_c(°C)$		55.66	16.87	105.70	25.96
Analytical-Analytical	$\phi_1(mW)$	Eq (16)	-9.91	-15.26	-4.81	-6.45
		Eq (17)	-9.91	-15.26	-4.98	-6.76
	$\phi_2(mW)$	Eq (16)	9.91	17.76	15.00	26.58
		Eq (17)	9.91	17.76	14.84	26.27
	$T_c(°C)$	Eq (16)	54.57	16.54	104.6	25.63
		Eq (17)	56.75	17.20	106.7	26.29

7. Conclusion:

In this work, it was shown that it is possible to use the 'contact resistance' concept to describe solid-solid contact with heat sources. This is done by using the notion of heat transfer partition coefficient. For electrothermal problems, we demonstrated that the partition coefficient is a constant equal to ½ whatever the system's geometrical configuration.

Numerical simulations were carried out for various thermal contact configurations with different cases. The excellent agreement between the numerical and analytical results demonstrates the validity of the proposed approach, which also allows to obtain the interface temperature using a simple thermal-electrical analogy. The deviation between Numerical and analytical results comes mainly from the calculation of the constriction resistances.

Nomenclature

Latin symbols

T	Temperature, K
Q	Rate of heat generation, W
S	Surface, m²
R	Thermal resistance, K/W
V	Volume, m^3
s	Curvilinear coordinate, m
g	Volumetric heat generation rate, W/m^3
e	Wall thickness, m
U	Electrical potential, V

Greek symbols

ϕ	Heat transfer rate, W
λ	Thermal conductivity, W/(m K)
ρ_e	Electrical resistivity, Ωm
β	Partition coefficient
α	heat generation factor
φ_g	the total rate of heat generation (W)

Subscripts and superscripts

in	inlet
out	outlet
i	internal
e	external
m	medium
a	asperity
f	fluid

Appendix 1:

To demonstrate that $A = C$ and $B = D$ (see figure 5), we only need to consider the hypothesis of a fully developed constriction, i.e. the heat flux in l_2 and l_1 is uniform (l_1 and l_2 are sufficiently larger than b). With reference to figure 5, we can write:

$$T_1 - A = R_{m1i}\phi_i = R_{m1i}\varphi_i S_i = \frac{l_1}{\lambda_1 S_i}\varphi_i S_i = \frac{l_1}{\lambda_1}\varphi_i$$

$$T_1 - C = R_{m1e}\phi_e = R_{m1e}\varphi_e S_e = \frac{l_1}{\lambda_1 S_e}\varphi_e S_e = \frac{l_1}{\lambda_1}\varphi_e$$

Or $\varphi_i = \varphi_e$ (uniform heat flux)

Therefore $A = C$. In a similar manner, we can demonstrate that $B = D$.

Appendix 2:

I. Calculations of the heat transfer rates and the interface temperature ($\boldsymbol{T_1 = T_2 = 0}$ with heat source)

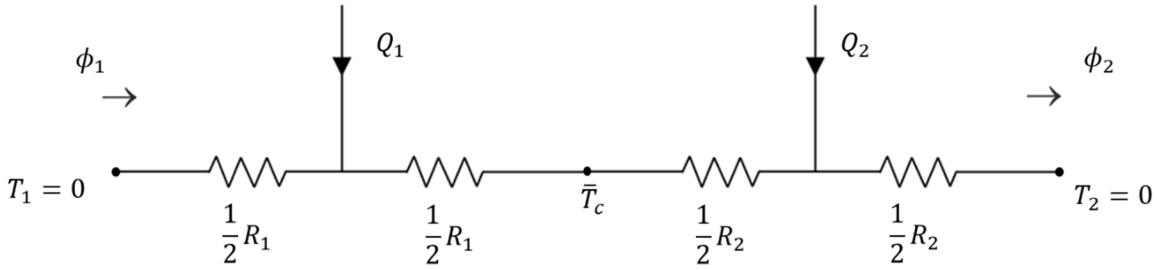

$$\phi_1 = -Q_1\frac{R_1 + 2R_2}{2(R_1 + R_2)} - Q_2\frac{R_2}{2(R_1 + R_2)}$$

$$\phi_2 = Q_1\frac{R_1}{2(R_1 + R_2)} + Q_2\frac{2R_1 + R_2}{2(R_1 + R_2)}$$

$$Q_1 = \frac{R_1^e}{R_1^e + R_2^e}Q \quad and \quad Q_2 = \frac{R_2^e}{R_1^e + R_2^e}Q$$

The superscript e stands for electrical resistance. Knowing that

$$R_1^e = \rho_1\lambda_1 R_1$$

And

$$R_2^e = \rho_2 \lambda_2 R_2$$

Substituting and rearranging we obtain the heat transfer rates:

$$\phi_1 = -\frac{Q}{2}\left[\frac{\rho_1\lambda_1 R_1^2 + \rho_2\lambda_2 R_2^2 + 2\rho_1\lambda_1 R_1 R_2}{(R_1+R_2)(\rho_1\lambda_1 R_1 + \rho_2\lambda_2 R_2)}\right]$$

$$\phi_1 = \frac{Q}{2}\left[\frac{\rho_1\lambda_1 R_1^2 + \rho_2\lambda_2 R_2^2 + 2\rho_2\lambda_2 R_1 R_2}{(R_1+R_2)(\rho_1\lambda_1 R_1 + \rho_2\lambda_2 R_2)}\right]$$

And the interface temperature

$$T_c = \frac{R_1 R_2 (Q_1+Q_2)}{2(R_1+R_2)} = \frac{Q}{2\left(\frac{1}{R_1}+\frac{1}{R_2}\right)}$$

In the last expression, we can see that the interface temperature depends only on the rate of heat generation

II. Calculations of the heat transfer rates and the interface temperature ($T_1 \neq T_2$ without heat source)

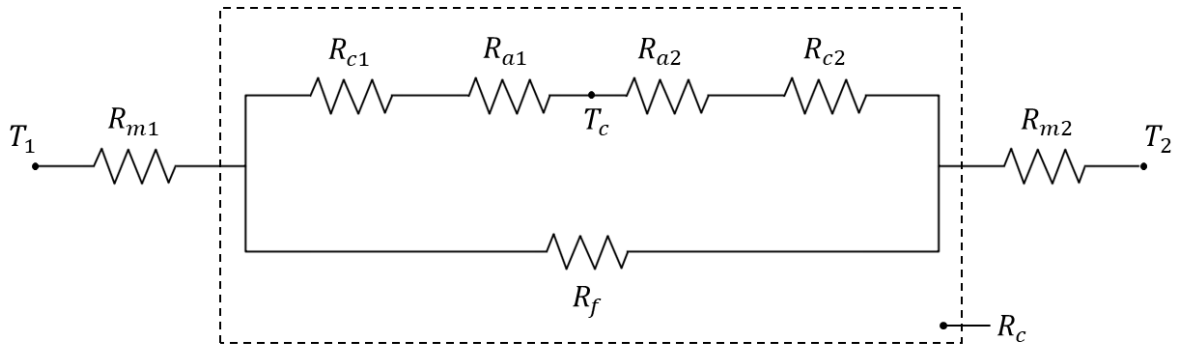

$$\phi = \frac{T_1 - T_2}{R_T} = \frac{\Delta T}{R_T}$$

With

$$R_T = R_{m1} + R_{m2} + \frac{(R_{c1}+R_{a1}+R_{c2}+R_{a2})R_f}{R_{c1}+R_{a1}+R_{c2}+R_{a2}+R_f}$$

We can also write

$$T_c = \frac{\Delta T}{R_T}\left[R_{m2} + \frac{(R_{c2}+R_{a2})R_f}{R_{c1}+R_{a1}+R_{c2}+R_{a2}+R_f}\right]$$

In the case where medium 1 and medium 2 have identical geometrical parameters:

$$R_{m1} = \frac{K}{\lambda_1} \quad , \quad R_{m2} = \frac{K}{\lambda_2}$$

$$R_{c1} + R_{a1} = \frac{K'}{\lambda_1} \quad , \quad R_{c2} + R_{a2} = \frac{K'}{\lambda_2}$$

Let's consider $R_u = R_{c1} + R_{a1} + R_{c2} + R_{a2} + R_f$

289 Therefore

290 $$R_T = (R_{m1} + R_{m2})\left[1 + \frac{\frac{R_{c1} + R_{a1} + R_{c2} + R_{a2}}{R_{m1} + R_{m2}} R_f}{R_u}\right]$$

291 And

292 $$T_c = \Delta T \frac{R_{m2}}{R_{m1} + R_{m2}} \left[\frac{1 + \frac{\frac{R_{c2} + R_{a2}}{R_{m2}} R_f}{R_u}}{1 + \frac{\frac{R_{c1} + R_{a1} + R_{c2} + R_{a2}}{R_{m1} + R_{m2}} R_f}{R_u}}\right]$$

293 With

294 $$\frac{R_{c2} + R_{a2}}{R_{m2}} = \frac{K'}{\lambda_2} \cdot \frac{\lambda_2}{K} = \frac{K'}{K}$$

295 And

296 $$\frac{R_{c1} + R_{a1} + R_{c2} + R_{a2}}{R_{m1} + R_{m2}} = \frac{\frac{K'}{\lambda_1} + \frac{K'}{\lambda_2}}{\frac{K}{\lambda_1} + \frac{K}{\lambda_2}} = \frac{K'}{K}$$

297 Thus

298 $$T_c = \Delta T \frac{R_{m2}}{R_{m1} + R_{m2}} \left[\frac{1 + \frac{K'}{K}\frac{R_f}{R_u}}{1 + \frac{K'}{K}\frac{R_f}{R_u}}\right]$$

299 $$T_c = \Delta T \frac{R_{m2}}{R_{m1} + R_{m2}}$$

300 In the last expression, we can see that the interface temperature does not depend on R_f (fluid
301 resistance).

302 **References**

303 1. Kato, T., & Fujii, H. (1999). Energy partition in conventional surface grinding. *Journal of*
304 *Manufacturing Science and Engineering*, *121*(3), 393-398.
305 2. Chandraeker, S., Farris, T. N., Hebbar, R. R., & Hucker, S. (1994). Thermal aspects of surface
306 finishing processes. *ASM International, Member/Customer Service Center, Materials Park, OH*
307 *44073-0002, USA, 1994.*, 152-157.
308 3. Grzesik, W. (1998). The role of coatings in controlling the cutting process when turning with coated
309 indexable inserts. *Journal of Materials Processing Technology*, *79*(1-3), 133-143.
310 4. Grzesik, W., & Nieslony, P. (2003). A computational approach to evaluate temperature and heat
311 partition in machining with multilayer coated tools. *International Journal of Machine Tools and*
312 *Manufacture*, *43*(13), 1311-1317.
313 5. Kulchytsky-Zhyhailo, R., & Yevtushenko, A. (1998). Axi-symmetric contact problem with frictional
314 heating for thermally nonlinear sliders. *International journal of mechanical sciences*, *40*(11), 1133-
315 1143.

6. Kulchytsky-Zhyhailo, R. (2001). A simplified solution for three-dimensional contact problem with heat generation. *International journal of engineering science*, *39*(3), 303-315.
7. Pauk, V., & Yevtushenko, A. (1997). Periodical contact problems for a half-space involving frictional heating. International journal of mechanical sciences, 39(1), 87-95.
8. Pauk, V. J. (1999). Plane contact problem for a layer involving frictional heating. *International journal of heat and mass transfer*, *42*(14), 2583-2589.
9. Grylitsky, D. V., & Pauk, V. J. (1995). Some quasistationary contact problems for half-space involving heat generation and radiation. *International journal of engineering science*, *33*(12), 1773-1781.
10. Yevtushenko, A. A., & Kulchytsky-Zhyhailo, R. D. (1995). Axi-symmetrical transient contact problem for sliding bodies with heat generation. *International journal of solids and structures*, *32*(16), 2369-2376.
11. Mazo, L., Cassagne, B., Badie-Levet, D., & Bardon, J. P. (1978). Etude des conditions de liaison thermique dans le cas du frottement sec métalplastique. *Rev. Gén. Therm*, *204*, 919-933.
12. Kulchytsky-Zhyhailo, R. D., & Yevtushenko, A. A. (1997). Thermoelastic contact problems with frictional heating and convective cooling. *International journal of engineering science*, *35*(3), 211-219.
13. Komanduri, R., & Hou, Z. B. (2001). Analysis of heat partition and temperature distribution in sliding systems. *Wear*, *251*(1-12), 925-938.
14. Komanduri, R., & Hou, Z. B. (2001). Thermal analysis of dry sleeve bearings—a comparison between analytical, numerical (finite element) and experimental results. *Tribology International*, *34*(3), 145-160.
15. Barber, J. R. (1967). Distribution of heat between sliding surfaces. *Journal of Mechanical Engineering Science*, *9*(5), 351-354.
16. Kounas, P. S., Dimarogonas, A. D., & Sandor, G. N. (1972). The distribution of friction heat between a stationary pin and a rotating cylinder. *Wear*, *19*(4), 415-424.
17. Levytskyi, V. P., & Onyshkevych, V. M. (1996). Plane contact problem with heat generation account of friction. *International journal of engineering science*, *34*(1), 101-112.
18. Ciavarella, M., Johansson, L., Afferrante, L., Klarbring, A., & Barber, J. R. (2003). Interaction of thermal contact resistance and frictional heating in thermoelastic instability. *International Journal of Solids and Structures*, *40*(21), 5583-5597.
19. Bardon, J. P. (1994). Bases physiques des conditions de contact thermique imparfait entre milieux en glissement relatif. *Revue générale de thermique*, *33*(386).
20. Chantrenne, P., & Raynaud, M. (1997). A microscopic thermal model for dry sliding contact. *International journal of heat and mass transfer*, *40*(5), 1083-1094.
21. Bauzin, J. G., & Laraqi, N. (2004). Simultaneous estimation of frictional heat flux and two thermal contact parameters for sliding contacts. *Numerical Heat Transfer, Part A: Applications*, *45*(4), 313-328.
22. Laraqi, N. (1992). Contact temperature and flux partition-coefficient of heat generated by dry friction between 2 solids-new approach to flux generation. *International Journal of Heat and Mass Transfer*, *35*(11), 3131-3139.
23. Guillot, E., Bourouga, B., Garnier, B., & Dubar, L. (2007, April). Experimental study of thermal sliding contact with friction: application to high speed machining of metallic materials. In *AIP Conference Proceedings* (Vol. 907, No. 1, pp. 1263-1268). AIP.
24. Chantrenne, P., & Raynaud, M. (2001). Study of a macroscopic sliding contact thermal model from microscopic models. *International journal of thermal sciences*, *40*(7), 603-621.
25. Han, Z., Orozco, J., Indacochea, J. E., & Chen, C. H. (1989). Resistance spot welding: a heat transfer study. *Welding journal*, *68*(9), 363s-371s.

26. Cho, H. S., & Cho, Y. J. (1989). A study of the thermal behavior in resistance spot welds. *Welding Journal*, *68*(6), 236s-244s.
27. Khan, J. A., Xu, L., Chao, Y. J., & Broach, K. (2000). Numerical simulation of resistance spot welding process. *Numerical Heat Transfer: Part A: Applications*, *37*(5), 425-446.
28. Wang, S. C., & Wei, P. S. (2001). Modeling dynamic electrical resistance during resistance spot welding. *Journal of heat transfer*, *123*(3), 576-585.
29. Le Meur, G., Bourouga, B., & Dupuy, T. (2003). Measurement of contact parameters at electrode/sheet interface during resistance spot welding process. *Science and technology of welding and joining*, *8*(6), 415-422.
30. Le Meur, G., Bourouga, B., & Bardon, J. P. (2006). Microscopic analysis of interfacial electrothermal phenomena—definition of a heat generation factor. *International journal of heat and mass transfer*, *49*(1-2), 387-401.
31. Feulvarch, E., Robin, V., & Bergheau, J. M. (2004). Resistance spot welding simulation: a general finite element formulation of electrothermal contact conditions. Journal of Materials Processing Technology, 153, 436-441.
32. Rogeon, P., Carre, P., Costa, J., Sibilia, G., & Saindrenan, G. (2008). Characterization of electrical contact conditions in spot welding assemblies. Journal of Materials Processing Technology, 195(1-3), 117-124.
33. Rogeon, P., Raoelison, R., Carre, P., & Dechalotte, F. (2009). A microscopic approach to determine electrothermal contact conditions during resistance spot welding process. *Journal of Heat Transfer*, *131*(2), 022101.
34. Degiovanni, A. G. M. L. A., Sinicki, G., Gery, A., & Laurent, M. (1984). Un modèle de résistance thermique de contact en régime permanent. *Revue générale de thermique*, *23*(267), 161-175.
35. Degiovanni, A., & Moyne, C. (1989). Résistance thermique de contact en régime permanent: influence de la géométrie de contact. *Revue générale de thermique*, *28*(334), 557-564.
36. Degiovanni, A., Remy, B., & Andre, S. (2003). Thermal resistance of a multi-constrictions contact: A simple model. *International journal of heat and mass transfer*, *46*(19), 3727-3735.
37. El Maakoul, A., Moyne, C., & Degiovanni, A. (2019). A general approach to solve heat conduction problems with internal heat sources using resistance and quadrupole concepts. *International Journal of Heat and Mass Transfer*, *129*, 793-800.
38. Maillet, D. (2000). Thermal quadrupoles: solving the heat equation through integral transforms. John Wiley & Sons Inc.